This is a repository copy of *A survey of the Wolf-Rayet population of the barred, spiral galaxy NGC 1313*.

White Rose Research Online URL for this paper:
http://eprints.whiterose.ac.uk/138886/

Version: Published Version

Article:

eprints@whiterose.ac.uk
https://eprints.whiterose.ac.uk/

A survey of the Wolf–Rayet population of the barred, spiral galaxy NGC 1313[★]

L. J. Hadfield† and P. A. Crowther

Department of Physics and Astronomy, University of Sheffield, Hounsfield Road, Sheffield S3 7RH

ABSTRACT

We present a VLT/FORS1 survey of Wolf–Rayet (WR) stars in the spiral galaxy NGC 1313. In total, 94 WR candidate sources have been identified from narrow-band imaging. Of these, 82 have been spectroscopically observed, for which WR emission features are confirmed in 70 cases, one of which also exhibits strong nebular He II λ4686 emission. We also detect strong nebular He II λ4686 emission within two other regions of NGC 1313, one of which is a possible supernova remnant. Nebular properties confirm that NGC 1313 has a metal content $\log$(O/H) + 12 = 8.23 ± 0.06, in good agreement with previous studies. From continuum-subtracted Hα images we infer a global star formation rate of $0.6\,M_\odot\,\mathrm{yr}^{-1}$. Using template LMC WR stars, spectroscopy reveals that NGC 1313 hosts a minimum of 84 WR stars. Our census comprises 51 WN stars, including a rare WN/C transition star plus 32 WC stars. In addition, we identify one WO star which represents the first such case identified beyond the Local Group. The bright giant H II region PES 1, comparable in Hα luminosity to NGC 595 in M 33, is found to host a minimum of 17 WR stars. The remaining photometric candidates generally display photometric properties consistent with WN stars, such that we expect a global WR population of $\sim$115 stars with N(WR)/N(O) $\sim$ 0.01 and N(WC)/N(WN) $\sim$ 0.4.

Key words: stars: Wolf–Rayet – galaxies: individual: NGC 1313.

1 INTRODUCTION

Wolf–Rayet (WR) stars are evolved, He-burning stars that are descended from the most massive O stars. They have a profound influence on their surroundings since intense stellar winds continually interact with their local environment returning mechanical energy and processed material to the interstellar medium. In recent years, WR stars have received renewed interest since they are believed to be the immediate precursors of Type Ib/c supernovae (SNe) and long γ-ray bursts (Crowther 2007).

WR stars are characterized by strong, broad, emission lines of nitrogen (WN), carbon (WC) or oxygen (WO). Their unique spectral appearance allows WR stars to be readily identified in external galaxies and have been detected as individual stars in nearby galaxies (e.g. Massey & Johnson 1998) and in the integrated starlight of more distant galaxies (Schaerer, Contini & Pindao 1999). WR stars are expected to be present within instantaneous bursts between 3 and 5 Myr, such that they trace recent star formation.

The advent of 8-m class telescopes has allowed WR surveys to move beyond the Local Group, with recent work proving very successful at locating large numbers of WR stars in nearby (<5 Mpc) galaxies (Schild et al. 2003; Hadfield et al. 2005). Using a combination of narrow-band imaging sensitive to WR emission features, candidates may be readily identified in external galaxies, with follow-up spectroscopy establishing their nature. Consequently, the WR population of several, nearby galaxies have been studied, increasing the statistics of WR populations across a broad range of metallicities. In addition, since WR stars are expected to be the immediate precursors of SNe and γ-ray bursts, it is vital that we map the WR population in nearby galaxies.

NGC 1313 is an isolated, face-on SB(s)d spiral situated at a distance of 4.1 Mpc (Méndez et al. 2002). With a reported oxygen abundance of $\log$(O/H) + 12 $\sim$ 8.3 (Walsh & Roy 1997), the properties of NGC 1313 are reminiscent of irregular Magellanic-type galaxies, plus late-type spirals such as NGC 300 and M 33, such that one might expect NGC 1313 to host a substantial WR population.

Previous studies of the stellar content of NGC 1313 have utilized high-resolution *Hubble Space Telescope* (*HST*) broad-band photometry (Larsen 2004; Pellerin et al. 2007). With regards to the WR population, no direct investigation into the global WR population has been conducted, although signatures of WR stars have been detected in several bright H II regions within NGC 1313 (Walsh & Roy 1997).

This paper is structured as follows. The observations and data reduction techniques used in this analysis are described in Section 2. In Section 3, we present nebular properties for several regions within NGC 1313. The WR population and global content is examined in Sections 4 and 5. Finally we discuss and summarize our results in Section 6.

2 OBSERVATIONS AND DATA REDUCTION

NGC 1313 has been observed with the ESO Very Large Telescope UT2 (Kueyen) and Focal Reduced/Low-dispersion Spectrograph #1 (FORS1). The data were obtained using the standard resolution collimator which covers a 6.8×6.8-arcmin^2 field of view, with a plate scale of 0.2 arcsec pixel^{-1}. Photometric observations of NGC 1313 were obtained on 2004 October 12, with spectroscopic data following in 2004 November and 2005 November–December. Details of the observations can be found in Table 1.

To supplement our VLT/FORS1 observations, we have retrieved archival *HST* Advanced Camera for Surveys (ACS) Wide Field Camera (WFC) images of NGC 1313 obtained with the F435W and F555W filters, at three different pointings of NGC 1313. All observations comprise a 680-s exposure and were obtained for programme ID GO 9774 (PI S. S. Larsen). At the distance of NGC 1313, the spatial scale of ACS/WFC is 1.0 pc pixel^{-1} (0.05 arcsec pixel^{-1}).

2.1 Imaging and photometry

FORS1 was used on the night of 2004 October 12 to obtain narrow-band images centred on $\lambda4684$ and $\lambda4781$ [full width at half-maximum (FWHM) = 66 and 68 Å, respectively]. In addition, narrow-band on- and off-Hα images ($\lambda6563, 6665$ Å, FWHM = 61, 65 Å) were acquired along with broad-band *B* images. All images were taken in photometric conditions and in seeing conditions of 0.6–0.9 arcsec.

Images were reduced following standard reduction procedures (i.e. debiased, flat-field corrected and cosmic ray cleaned) using IRAF and STARLINK packages.

We present broad-band *B* and continuum-subtracted Hα images of the surveyed region in Fig. 1, clearly illustrating the barred-spiral structure of NGC 1313. The net Hα image of NGC 1313 shows that the nebular emission within NGC 1313 is mainly concentrated along the spiral arms, with the central bar relatively faint in ionized gas. In addition, NGC 1313 contains three 'satellite' H II regions to the

Table 1. VLT/FORS1 observation log for NGC 1313.

Date	Filter/ mask ID	Exposure time (s)	DIMM seeing (arcsec)
	Imaging		
2004 October 12	Bessel B	60, 300	0.9
	$\lambda4684, 4871$	1500	0.65, 0.75
	$\lambda6665, 6563$	300	0.62–0.69
	Spectroscopy		
2004 November 14	Mask D	3×600	0.6–0.7
	Mask E	3×800	0.6–0.8
	Mask F	3×800	0.5–0.8
2005 November 25	Mask G	3×800	0.7
2005 November 27	Mask A	3×300	0.5
2005 December 08	Mask B	3×300	0.7–0.8
	Mask C	3×600	0.7

Figure 1. VLT FORS1 broad-band *B* (top) and continuum-subtracted Hα (bottom) frames of the surveyed region of NGC 1313. The orientation of the images is marked and the field of view of each frame is 6.8×6.8 arcmin^2.

south of the nucleus. In total, Marcelin & Gondoin (1983) have catalogued 375 H II regions within NGC 1313.

Photometry of individual sources within NGC 1313 was performed using the IRAF point spread function (PSF)-fitting routine DAOPHOT. Landolt (1992) photometric standard fields Mark A and PG 2331+055 (containing a total of seven photometric standard stars) were observed for absolute calibration of *B*-band images. Photometric zero-points were found to differ by 0.7 mag, so we have recalibrated our photometry using *HST*/ACS F435W images. For the narrow-band images, photometric zero-points were obtained by observing the spectrophotometric standard GD 71 ($m_B = 12.8$ mag).

A number of sources do not appear point-like on our VLT/FORS1 images and have therefore been excluded from our DAOPHOT photometry.

2.2 Candidate selection

WR candidate stars were identified by searching for He II $\lambda4686$/C III $\lambda4650$ emission (at $\lambda4684$) relative to the

continuum ($\lambda4781$). As noted by Hadfield et al. (2005), candidate He II emission regions are most readily identified by 'blinking' the individual $\lambda4684$ and $\lambda4781$ images along with a difference image (obtained by subtracting the $\lambda4781$ frame from the $\lambda4684$ image). In total, 94 $\lambda4684$ emission-line candidates were identified in NGC 1313. These are listed in Table A2 in Appendix A.

For the majority of our targets ($\sim$90 per cent) we have obtained photometry in at least the $\lambda4684$ filter. For $\sim$30 per cent of these regions it was not possible to obtain a $\lambda4871$ magnitude since the object was below the detection limit of our photometry. For five regions PSF photometry was not possible since they were located in extremely crowded regions of the galaxy. Sources which were not detected in our images are given an upper limit in Table A2.

2.3 MOS spectroscopy

FORS1 Multi-Object Spectroscopy (MOS) of candidate WR regions within NGC 1313 was undertaken during 2004 November and 2005 November–December in seeing conditions between 0.5 and 0.8 arcsec. Spectra were acquired using a 0.8-arcsec slit and the 300V grism (centred on 5850 Å), resulting in a dispersion of 3 Å pixel^{-1} and resolution of $\sim$8 Å (as measured from comparison arc lines).

In total, 82 of the 94 candidates have been spectroscopically observed in seven different MOS mask configurations, which were labelled A to G (see Table 2). To maximize signal-to-noise ratio (S/N), candidates were ranked based on the observed $\lambda4684$ excess and then grouped according to continuum brightness. Exposure times ranged between 900 s for our brighter candidates ($m_B \sim$ 18 mag) and 2400 s for the fainter targets ($m_B \gtrsim$ 20 mag). The blue ($\sim$4500 Å) continuum S/N ranged from $\sim$50 for the brighter sources to $\lesssim$1 for the very faint cases. Nevertheless, blue WR features were generally detected at the 20σ level.

Positional restrictions typically permitted $\sim$15 candidates to be observed simultaneously using FORS1. Since MOS spectroscopy allows the spectra of 19 targets to be obtained per MOS mask, we have supplemented our analysis by observing nine H II regions within NGC 1313.

For brevity we have assigned #1–94 and H1–9 nomenclature to our WR candidates and H II regions, respectively. Positional and photometric information is presented in Tables A1 and A2 in Appendix A. Additional information (i.e. spectral classification etc.) is included for those regions that were included in spectroscopic

follow-up investigations. FORS1 narrow-band $\lambda4684$ finding charts can be found in the (electronic only) Appendix, Figs B1–B10.

Data were prepared and processed using standard techniques and IRAF and STARLINK packages, i.e. bias subtracted, flat-field corrected, extracted and flux/wavelength calibrated, with care being taken during the extraction process to minimize contamination from neighbouring sources. The wavelength coverage of individual candidates is dependent on their location on the CCD, but for the majority of targets a spectral coverage of 3500–7500 Å was achieved.

The spectrophotometric standards LTT 3218 and GD 108 were observed in order to relatively flux calibrate the spectra. Slit-loss corrections are estimated to be of the order of $\sim$5–20 per cent for seeing conditions between 0.5 and 0.8 arcsec. FORS1 has an atmospheric dispersion compensator and so slit-losses will be independent of wavelength. Consequently, observed data have been uniformly scaled by up to 20 per cent to match the conditions in which they were obtained.

For very faint cases, no continuum was present on the raw 2D frame and identification was made solely on the presence of emission features. A nearby continuum source was used as a trace during extraction.

3 NEBULAR ANALYSIS

Here we derive the nebular properties of several regions within NGC 1313. Of the 82 candidate and nine H II regions spectroscopically observed, the strength of the [O III] $\lambda4363$ line was detected at the 5σ level in only six regions permitting a determination of T_e. These are NGC 1313 #14 and 85, H1, H2, H3 and H5.

The nebular analysis was performed using the STARLINK package DIPSO with line fluxes being determined using the ELF (emission-line fitting) routine to fit Gaussian line profiles to the spectral features. Observed and dereddened line fluxes are presented in Table 2.

3.1 Interstellar extinction

The interstellar extinction towards NGC 1313 has been estimated using the observed Hα/Hβ line ratios (accounting for nearby [N II] emission) for the nine H II regions observed in this analysis (see Table A2). Assuming Case B recombination theory for electron densities of 10^2 cm^{-3} and a temperature of 10^4 K (Hummer & Storey 1987), we calculate total E_{B-V} values ranging between 0.19 and 0.56 mag, with an average $E_{B-V}^{\mathrm{TOT}} = 0.29 \pm 0.04$ mag.

Table 2. Observed (F_λ) and dereddened (I_λ) nebula line fluxes of six H II regions within NGC 1313. Line ratios are normalized to H$\beta = 100$ and we present the observed and dereddened Hβ line flux in the penultimate row ($\times 10^{-13}$ erg s^{-1} cm^{-2}).

λ_{rest}	ID	#14		#85		H1		H2		H3		H4	
		F_λ	I_λ	F_λ	I_λ	F_λ	I_λ	F_λ	I_λ	F_λ	I_λ	F_λ	I_λ
3727	[O II]	133.3	171.6	116.2	143.9	230.0	307.0	216.7	254.7	141.2	251.7	306.4	114.4
4363	[O III]	2.6	3.0	3.1	3.4	2.9	3.3	4.8	5.2	5.0	2.9	3.2	4.5
4861	Hβ	100	100	100	100	100	100	100	100	100	100	100	100
4959	[O III]	150.0	146.4	169.0	165.9	107.0	104.1	125.0	123.1	182.9	127.6	125.2	186.6
5007	[O III]	435.0	420.0	503.5	488.7	330.0	317.0	375.0	366.6	561.0	372.4	362.4	577.5
6563	Hα	391.7	286.0	373.4	286.0	410.0	286.0	350.0	286.0	286.0	365.5	286.0	371.1
6583	[N II]	16.1	11.7	12.6	9.6	33.0	22.9	16.7	13.6	10.5	32.8	25.6	13.7
6717	[S II]	15	10.7	14.8	11.1	33.0	22.5	17.4	14.0	11.0	47.9	36.9	14.5
6731	[S II]	11.2	8.0	11.0	8.3	25.1	17.1	13.2	10.6	8.4	33.1	25.5	11.1
7330	[O II]	4.4	2.9	4.8	3.4	11.0	6.9	10.0	7.7	2.8	6.9	5.0	3.9
4861	Hβ	18.0	48.1	17.3	39.8	1.0	3.0	1.2	2.3	21.9	2.9	6.2	9.7
E_{B-V}		0.29		0.25		0.34		0.19		0.23		0.24	

Underlying Hα,Hβ absorption from early-type stars is expected to be of the order of $W_\lambda \sim 2$ Å. Observed Hα and Hβ equivalent widths are approximately 1550 and 150 Å, respectively, suggesting that underlying stellar absorption is negligible.

Foreground Galactic redding towards NGC 1313 is estimated to be $E_{B-V} = 0.10$ mag (Schlegel, Finkbeiner & Davis 1998), suggesting a modest average internal extinction of $E_{B-V} = 0.19 \pm 0.05$ mag for NGC 1313. All reddening corrections were made following a standard Seaton (1979) extinction law and $A_V/E_{B-V} = 3.1$.

A subset of the regions presented here are associated with the bright H II regions studied by Pagel, Edmunds & Smith (1980) and Walsh & Roy (1997). We obtain $E_{B-V} = 0.23$ mag for H3, substantially lower than $E_{B-V} = c(H\beta)/1.64 = 0.71$ mag derived by Walsh & Roy (their no. 20). Considerable differences are also obtained for the other regions in common with this study. Overall, both Pagel et al. and Walsh & Roy imply a moderately high extinction towards NGC 1313, with an average $E_{B-V} = 0.47$ mag (cf. $E_{B-V} = 0.29$ mag obtained here). However, a direct comparison is not straightforward since the specific region sampled in the different studies is known to differ (i.e. H II region no. 20 from Walsh & Roy is associated with three subregions observed in our analysis).

3.2 Electron densities and temperatures

Electron densities (N_e) and temperatures (T_e) were determined for the six H II regions from diagnostic line ratios presented in Table 2, using the five-level atom calculator TEMDEN.

Electron densities were calculated assuming a constant T_e of 10 000 K. For five regions investigated we derive $N_e \sim 100$ cm^2, typical of that expected for H II regions. For H3 a direct determination of N_e was not possible since the [S II] 6717/6731 Å line ratio is below the limits of the line diagnostic. Consequently we have adopted $N_e = 50$ cm^2 for temperature and abundance calculations for this region.

Estimates of the electron temperatures have been derived using the [O II] 3727/7330 Å and [O III] (4959+5007)/4363 Å diagnostic ratios. For the majority of regions we find that T_e lies between 9500 and 12 000 K, except for H2 where we derive a slightly larger electron temperature of $\sim$13 000 K.

Errors on $T_e(O^+)$ were based on the 10 per cent measurement error estimated for the λ7330 Å while we assume that the 15 per cent formal error associated with [O III] 4363 Å dominates the uncertainty on $T_e(O^{2+})$.

3.3 Oxygen abundance

We have directly measured the O/H content of our six H II regions in NGC 1313 using the [O II] λ3727 and [O III] λ5007 nebular emission features along with associated electron temperatures and densities. Oxygen abundances were derived using the IRAF utility ionic. The total oxygen content for each region was computed assuming that $N(O)/N(H) = N(O^+)/N(H) + N(O^{2+})/N(H)$. Abundance estimates for individual H II regions are presented in Table 3.

We derive an average $12 + \log(O/H)$ for NGC 1313 of 8.23 ± 0.06. This agrees with 8.32 ± 0.08 from Walsh & Roy (1997) to within the quoted errors. Oxygen abundances derived here confirm that NGC 1313 is somewhat intermediate in metallicity between the Large (LMC) and Small (SMC) Magellanic Clouds for which $12 + \log(O/H) \sim 8.13$ and 8.37, respectively (Russell & Dopita 1990).

Our derived (O/H) abundances show no evidence for a radial dependence in agreement with previous findings of Walsh & Roy (1997) and Pagel et al. (1980). This probably results from the barred

Table 3. Electron temperature, density and oxygen abundance for six regions within NGC 1313.

Diagnostic	#14	#85	Region H1	H2	H3	H4
Density N_e (cm^{-3})						
λ6717/λ6731	80	80	100	100	(50)	100
	±50	±50	±60	±60		±60
Temperature T_e (K)						
λ3727/λ7330	9500	11 500	12 000	13 500	11 000	10 500
	±300	±500	±500	±500	±500	±400
$\frac{\lambda4959+\lambda5007}{\lambda4363}$	10 500	10 500	12 000	13 000	11 000	11 000
	±400	±400	±500	±600	±500	±500
Abundances						
O$^+$/H (×10^{-5})	7.2	3.0	7.8	3.1	13.4	4.5
	±0.8	±0.2	±0.9	±0.1	±1.6	±0.4
O^{2+}/H (×10^{-5})	13.5	15.8	6.6	5.5	8.2	14.4
	±3.9	±4.3	±1.5	±1.3	± 3.1	±4.2
O/H (× 10^{-5})	20.7	18.8	14.4	8.6	21.6	18.9
	±4.0	±4.3	±1.7	±1.3	±3.5	±4.2
12 + log(O/H)	8.32	8.27	8.16	7.93	8.34	8.27
	±0.07	±0.08	±0.04	±0.05	±0.06	±0.08
Average			8.23 ± 0.06			

nature of the galaxy, in which the bar provides an effective means of homogenizing the radial abundance gradients, as demonstrated by numerical simulations (Friedli, Benz & Kennicutt 1994).

3.4 Hα fluxes

We have measured net Hα fluxes for the 11 bright H II emission regions of NGC 1313 identified by Pagel et al. (1980) (denoted PES 1–11) plus the 'satellite' region 3 arcmin to the south-east of the nucleus (designated P#12 in Table 4).

Narrow-band Hα observations of galaxies suffer from contamination by nearby [N II] λλ6548, 6583 emission. For metal-rich spiral galaxies [N II] is expected to contribute 1/3 of Hα flux, decreasing to only 8 per cent for metal-poor irregulars (Kennicutt & Kent 1983). Indeed, for the six regions presented in Table 2, we estimate [N II]/Hα ~ 0.06 (assuming [N II] 6548/N II] 6583 ~ 3). Consequently, continuum-subtracted Hα fluxes have been corrected downwards by 6 per cent.

Where possible, we have derived an average extinction for these 12 bright H II regions using spectroscopy of individual sources in common with this study. For PES 7, 8 and 12, this was not possible since our spectra started redward of Hβ. For PES 2, 9 and 11 no spectra were available. For these regions, and for the galaxy as a whole, we have adopted our average total extinction of $E_{B-V} = 0.29$ mag.

For our assumed distance of 4.1 Mpc, we derive Hα luminosities for the bright H II regions in the range of 2.3×10^{38}–2.3×10^{39} erg s^{-1}. The brightest region (PES 1) has an ionizing flux comparable to that observed for NGC 595 in M 33, while the faintest region (PES 9) is more consistent with that observed for SMC N19 (Kennicutt 1984). For the entire galaxy we derive a Hα luminosity of 8.4×10^{40} erg s^{-1} which is comparable to $\sim$6500 O7V star equivalents, assuming a typical O7V star in the SMC has an ionizing output of 10^{49} erg s^{-1} (Hadfield & Crowther 2006).

Of course, the O stars in NGC 1313 will not be restricted to O7V spectral types, but will cover the entire spectral range. For continuous star formation it is hard to quantify the specific spectral-type

Table 4. Dereddened Hα fluxes and luminosities for the 12 primary H II regions within NGC 1313, including the 11 regions identified by Pagel et al. (1980) plus one satellite region 3 arcmin to the south-east of the nucleus. Observed fluxes have been derived from continuum-subtracted VLT/FORS1 images and have been corrected to account for nearby [N II] emission. Extinction corrections have been made using the average E_{B-V} derived from candidates present within each region. Values in parentheses correspond to regions where we adopted our average extinction. In the final row we present the integrated Hα properties for the galaxy as a whole. Lyman continuum ionizing fluxes (Q_0) have been estimated assuming the calibration of Kennicutt (1998).

Region	α	δ (J2000)	Ap (arcsec)	E_{B-V} (mag)	F(Hα) (erg s^{-1} cm^{-2})	L(Hα) (erg s^{-1})	log Q_0 (photons s^{-1})
PES 1	03:18:23.9	−66:28:47.7	20	0.12	8.7×10^{-13}	2.3×10^{39}	51.23
PES 2	03:18:38.0	−66:29:19.7	12	(0.29)	1.1×10^{-13}	4.3×10^{38}	50.50
PES 3	03:18:37.8	−66:29:34.2	10	0.25	4.5×10^{-13}	1.6×10^{39}	51.07
PES 4	03:18:16.8	−66:28:44.3	15	0.26	2.3×10^{-13}	8.5×10^{38}	50.79
PES 5	03:18:05.3	−66:30:27.1	6	0.37	3.1×10^{-13}	1.4×10^{39}	51.02
PES 6	03:18:03.2	−66:30:16.5	24	0.27	6.1×10^{-13}	2.3×10^{39}	51.22
PES 7	03:18:03.5	−66:33:32.3	18	(0.29)	8.4×10^{-14}	3.3×10^{38}	50.38
PES 8	03:17:39.2	−66:31:26.5	18	(0.29)	1.0×10^{-13}	4.1×10^{38}	50.47
PES 9	03:18:18.3	−66:29:02.2	12	(0.29)	6.0×10^{-14}	2.3×10^{38}	50.23
PES 10	03:18:42.2	−66:29:32.0	12	0.33	1.6×10^{-13}	6.9×10^{38}	50.70
PES 11	03:18:19.6	−66:28:43.5	22	(0.29)	1.7×10^{-13}	6.5×10^{38}	50.68
P#12	03:18:23.7	−66:32:55.9	20	0.29	0.9×10^{-13}	3.7×10^{38}	50.43
NGC 1313	03:18:14.9	−66:29:33.1	460	(0.29)	2.2×10^{-11}	8.5×10^{40}	52.79

distribution, but it is likely that the actual O star content of NGC 1313 is a factor of 2 higher, i.e. 13 000 stars. Indeed, the star formation rate (SFR) in the SMC implies ∼400 O7V equivalents (Kennicutt et al. 1995), yet the global star content may be as high as ∼1000 (Crowther 2007).

Using the Hα–SFR relation of Kennicutt (1998) we obtain a global SFR of $0.6 \, M_\odot \, \text{yr}^{-1}$, substantially lower than the previous Hα estimate of $1.4 \, M_\odot \, \text{yr}^{-1}$ (Ryder & Dopita 1994).

### 3.5 Nebular He II λ4686

Except for planetary nebulae, nebular He II λ4686 emission is not expected to be observed in 'normal' H II regions since O stars do not emit sufficient extreme ultraviolet photons ($\lambda < 228$ Å) to produce a significant He$^+$ ionizing flux. However, seven such H II regions have been identified within the Local Group (Garnett et al. 1991), five of which are associated with WR stars. Here, we have identified three regions within NGC 1313 which exhibit strong nebular He II λ4686 consistent with highly ionized nebulae.

The dereddened spectra of NGC 1313 #6, 19 and 74 are presented in Fig. 2. The broad stellar component and superimposed nebular He II λ4686 are clearly evident in #19, as is the presence of strong [Fe III] λ4658 and [Ar IV] λ4711 in #74. Table 5 lists derived properties of these three nebulae, along with those for known He II λ4686 nebulae in the Local Group.

The presence of a WN star within the spectrum of #19 would suggest that this is responsible for the hard ionizing photons, and based on the He II λ4686 stellar line flux we infer the presence of a single WN2–4 star (see Section 4). We derive a nebular $I(\lambda4686)/I(\text{H}\beta) = 0.25$, which is consistent with that observed for other metal-poor early-type WN stars (e.g. N79 in the LMC; Nazé et al. 2003b).

For the two regions in which WR stars were not detected, supernova remnants (SNRs) or X-ray sources are possible ionizing sources. In general, the distinction between photoionized and shocked regions is made using the [S II]/Hα ratio, with the dividing point being an empirical value based on observations of known SNRs. Typical H II regions have an observed [S II]/Hα ratio of ∼0.1 versus 0.5–1.0 observed in SNRs (Smith et al. 1993). A [S II]/Hα =
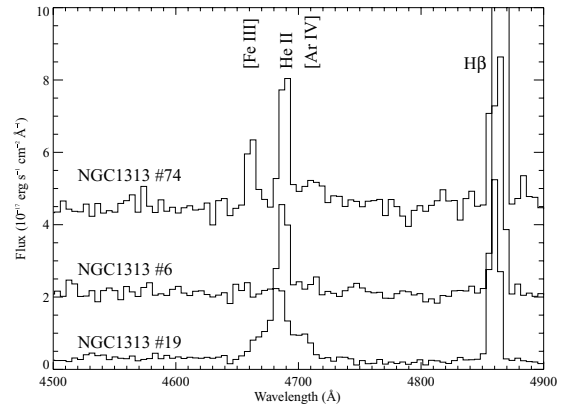
Figure 2. Dereddened ($E_{B-V} = 0.29$ mag) VLT/FORS1 spectra of NGC 1313 #6, 19 and 74, showing the presence of strong, narrow nebular He II λ4686. A broad WR He II emission is clearly evident in NGC 1313 #19. For clarity each spectrum has been successively offset by $1.5 \times 10^{-17} \, \text{erg s}^{-1} \, \text{cm}^{-2} \, \text{Å}^{-1}$.

0.4 is generally taken as the standard discriminator and is found to be independent of metallicity.

#74 appears to be consistent with known SNR since [S II]/Hα = 0.5. In addition, [O I] λλ6300, 6364 and [N II]λλ6548, 6583 are strong with respect to Hα also suggesting shock ionization. We therefore believe that #74 is a shocked SNR, instead of a photoionized H II region.

For #6, both [S II] and [N II] are observed to be much weaker than in #74, and with [S II]/Hα = 0.2 it is not consistent with an SNR. The absence of a hot WR star suggests possible similarities with N44C and N159 in the LMC, where the high excitation is linked to possible X-ray sources within the nebulae. To date, however, no bright ($L_X \geqslant 10^{38}$ erg s^{-1}) X-ray counterpart has been linked to #6 (Colbert, Petre & Ryder 1995; Miller et al. 1998).

4 SPECTROSCOPIC RESULTS

Of the 82 candidate regions spectroscopically observed we have identified broad WR emission features in 70 cases. Of the 12 cases

Table 5. Summary of properties of NGC 1313 #6, 19 and 74 and He II nebulae in the Local Group. Local He II have generally been spatially resolved into several components and so we list the full range of observed properties. The large [S II]/Hα observed for N79 corresponds to the SNR within the region.

Galaxy	Region	Ionizing source	Spectral type	$I(\lambda 4686)/$ $I(\mathrm{H}\beta)$	[S II]/ Hα	[N II]/ Hα	Reference
IC 1613	S3		WO3	0.23	0.05	0.02	2
NGC 1313	#19		WN2–4	0.25	0.16	0.08	7
SMC	N 76	AB7	WN4 + O6I(f)	0.16–0.24	0.02–0.14	0.02–0.05	5
LMC	N79	BAT99-2	WN2b(h)	0.21–0.56	0.10–0.25	0.05–0.26	6
LMC	N206	BAT99-49	WN4:b+O8V	0.08–0.10	0.09–0.22	0.08–0.13	5
MW	G2.4 + 1.4	WR102	WO2	0.4–1.2	0.08–0.8	0.5–1.0	3
NGC 1313	#74		SNR	0.11	0.50	0.92	7
NGC 1313	#6			0.27	0.17	0.07	7
LMC	N159	X-1	HMXB	0.05		0.24	1
LMC	N44C	X-5?	X-ray Neb?	0.02–0.14	0.06–0.26	0.03–0.35	4

References: (1) Garnett et al. (1991); (2) Kingsburgh & Barlow (1995); (3) Polcaro et al. (1995); (4) Garnett, Galarza & Chu (2000); (5) Nazé et al. (2003a); (6) Nazé et al. (2003b); (7) this paper.

where we did not detect broad WR emission, two sources displayed strong nebular He II λ4686 (see Section 3.5) and in four cases, the spectral coverage started longward of the He II λ4686 feature required for WN classification. Only six spectra showed no evidence for WR features, of which three were consistent with foreground late-type stars.

Prior to the present study, the WR population of NGC 1313 has not been directly investigated. Strong WR signatures have been detected in two of the H II regions investigated by Walsh & Roy (1997), their regions 3 and 28. Here, we can confirm the presence of WR stars in both these regions, although a quantitative comparison is not possible.

Optical spectral classification of WR stars is generally straightforward, since line diagnostic schemes are well defined (Smith, Shara & Moffat 1996; Crowther, De Marco & Barlow 1998). Indeed, for most regions distinguishing between WC (strong C IV λ5808), WN (strong He II λ4686) and WO (strong O VI λ3820) type stars was relatively straightforward.

For a refined classification of WN stars, we refer to Crowther & Hadfield (2006) who showed that Magellanic Cloud WN stars could be further divided into early (WN2–4), mid (WN5–6) and late (WN7–9) subtypes. We shall now discuss the WR content of NGC 1313 in detail.

4.1 WN population

In 44 spectra the emission-line features present are characteristic of nitrogen-rich (WN) WR stars, with strong He II λ4686. We have assigned a WN2–4 (WNE) or WN7–9 (WNL) subtype to each region if He II λ4686 is accompanied by N V λ4603–20 or N III λ4634–41, respectively. For cases where nitrogen emission was not detected, WNE subtypes were preferred for regions in which broad He II λ4686 (FWHM > 20 Å) was observed, otherwise a WNL subtype generally was assumed. WN5–6 stars, in which N V and N III emission is weak, are found to be exclusive to the cores of luminous H II regions within the LMC (e.g. 30 Doradus). NGC 1313 contains several such regions, to which we tentatively assign WN5–6 subtypes. Since these classifications cannot be spectroscopically confirmed, we note that the WN distribution of NGC 1313 may be atypical. Therefore, to reflect any possible ambiguity surrounding

Table 6. Global WR population of NGC 1313 inferred from spectroscopy using dereddened line fluxes and assuming a distance of 4.1 Mpc. The number of WR stars in each source has been estimated using the line luminosity calibrations, $\log L_{\mathrm{LMC}}$ (erg s^{-1}), of Crowther & Hadfield (2006) for LMC WR stars. The total inferred WR population adds up to more than the number of regions observed since several regions are believed to contain multiple WR stars.

| Subtype	WN2–4	WN5–6?	WN7–9	WN/C	WC4–5	WO
Line	λ4686	λ4686	λ4686	λ4686	λ5808	λ5808
$\log L_{\mathrm{LMC}}$	35.92	36.2	35.86	35.92	36.53	36.01
N(WR)	22	6	22	1	32	1

the classification of these regions, we have adopted WN5–6? subtypes in Table A2.

WN stars are known to exhibit a wide range of intrinsic properties (e.g. Schaerer & Vacca 1998; Crowther & Hadfield 2006) and converting between line luminosity and WR content leads to large uncertainties on derived populations. Consequently, we suggest a single WN star for each source unless the line luminosity formally suggests the presence of three or more stars.

For the majority of our WN sources, dereddened line fluxes are consistent with single LMC-like counterparts, assuming average He II λ4686 line luminosity calibrations of Crowther & Hadfield (2006) (see Table 6). The exceptions are sources NGC 1313 #33 and 58 where we estimate that three WN5–6 and three WN2–4 stars, respectively, are required to reproduce the observed He II line flux.

In Fig. 3(a) we compare early WN sources in NGC 1313 with a generic LMC WN2–4 template spectrum. The spectra shown are in general representative of the observed WNE stars and based on a spectral comparison we confirm that LMC WN2–4 templates are appropriate local analogues for WNE stars in NGC 1313. A similar comparison between late-type WN stars in NGC 1313 and a generic LMC WN7–9 template star is shown in Fig. 3(b).

From spectroscopy we estimate a total WN population of 50 stars. The subtype distribution is summarized in Table 6. For NGC 1313 #1 we quote a WR population of ⩾1WNE star in Table A2 since it was not possible to extract a reliable spectrum as the object was
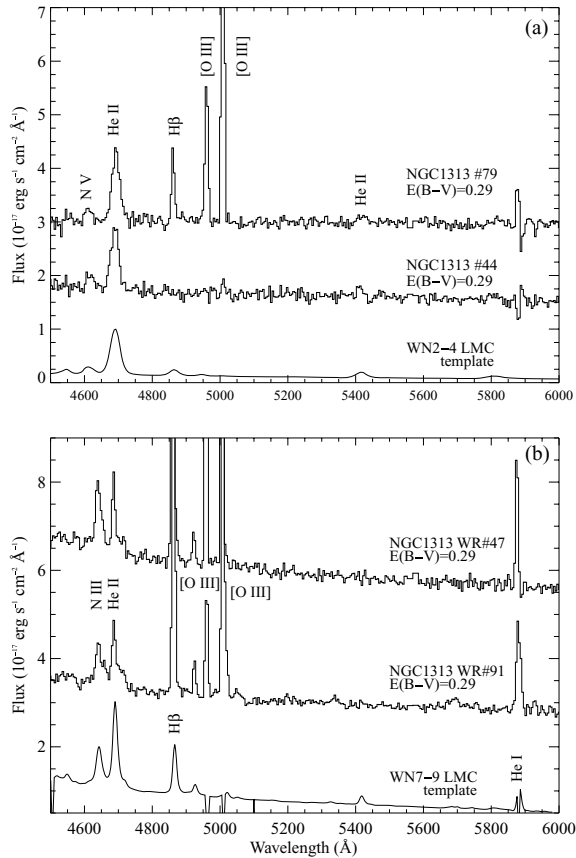
Figure 3. Dereddened spectral comparison between (a) early and (b) late WN regions in NGC 1313 and 'generic' optical spectra for single WN stars in the LMC (Crowther & Hadfield 2006). For clarity individual spectra have been offset by 2×10^{-17} erg s^{-1} cm^{-2}.

located at the edge of the slit. Broad He II is clearly present in the raw 2D image and with no evidence of WC features we identify a dominant WNE population.

4.2 WN/C stars

For one region, NGC 1313 #11, the observed spectral features are not consistent with normal WN or WC stars. In Fig. 4 we compare the dereddened FORS1 spectrum of #11 along with that of the LMC WN5–6/C4 star Brey 29 (BAT99-36) from Crowther, Smith & Willis (1995). Strong WC (C IV λ5808) and WN (He II λ4686, λ5411) features are clearly present in both stars. C III λ4650 is very weak and the relative strength of the N III λ4634–4640 and He II λ4686 suggests a WN5–6 classification, while strong C IV λ5808 suggests a WC4–5 classification. The similarity in spectral morphology to Brey 29 suggests a composite WN5–6/C4–5 classification for this source.

Transition WN/C stars are rare, and to date only six such stars have been identified within the Galaxy, plus two in the LMC. Since the total WR populations of the Galaxy and the LMC are 313 (van der Hucht 2006; Hadfield et al. 2007) and 134, respectively, we find that the total observed fraction of WN/C stars for each galaxy is ∼1–2 per cent. Indeed, this is comparable to observed statistics for NGC 1313, i.e. N(WN/C)/N(WR) = 1/84 ∼ 1 per cent.
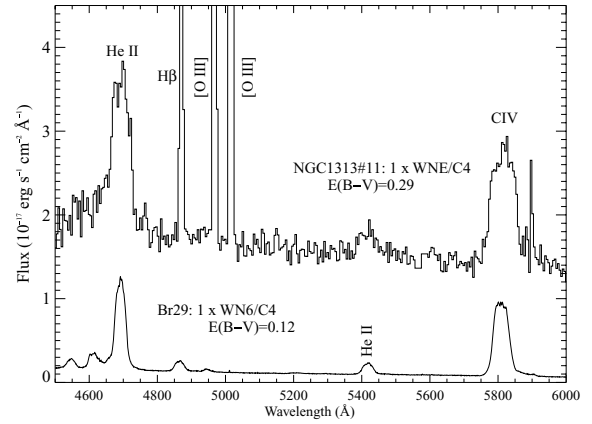
Figure 4. Dereddened spectroscopic comparison between NGC 1313 #11 and LMC WN/C star Brey 29 (BAT99-36). The spectrum of Brey 29 is taken from Crowther et al. (1995) and has been corrected for an extinction of $E_{B-V} = 0.12$ mag and scaled to the distance of NGC 1313.

4.3 The WC content

For 24 regions spectroscopically observed we have identified broad blue and red emission features, consistent with those expected from carbon-rich WR stars. C III λ5696 is very weak or absent in all 24 spectra whereas C IV λ5808 is present at the 20σ level, as illustrated in Fig. 5. Since WC stars are classified using the C III λ5696/C IV λ5808 line ratio (Smith, Shara & Moffat 1990), the absence of C III λ5696 suggests a WC4–5 subtype for all 24 regions.

For three regions, spectral coverage started longward of λ5000 and WC classification was assigned based solely on the C IV λ5808 detection. For the majority of sources, dereddened C IV λ5808 line luminosities are consistent with a single LMC-like WC4 star. For NGC 1313 #10, 48, 66 and 88 the observed line fluxes suggest the presence of two WC stars whereas we estimate a content of ∼3 WC4–5 stars for NGC 1313 #61 and 64.

For regions NGC 1313 #59 and 67, we find that the blue WR features cannot be reproduced by a population comprising solely of WC stars. In Fig. 6 we compare the dereddened, continuum-subtracted C IV λ5808 profile for #59 with that expected from an LMC-like, generic WC4 star at the distance of NGC 1313. The observed red feature is well reproduced by a single WC4–5 star. In the blue, a
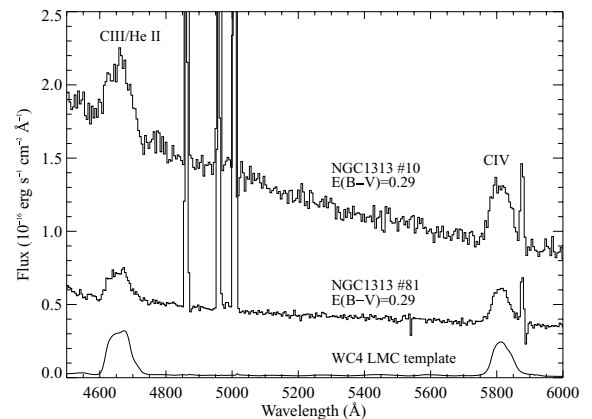
Figure 5. Dereddened spectral comparison between WC regions within NGC 1313 and 'generic' optical spectra for an LMC-like WC4 star (Crowther & Hadfield 2006). For clarity individual spectra have been offset by 0.1×10^{-16} erg s^{-1} cm^{-2} Å^{-1}.
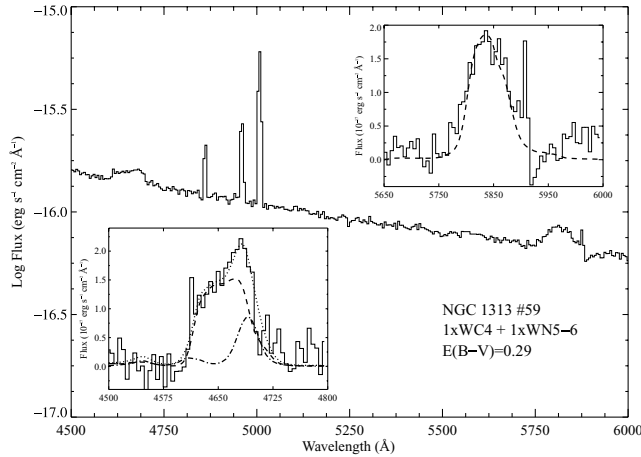
Figure 6. Dereddened, velocity-corrected VLT/FORS1 optical spectrum of NGC 1313 #59. Also shown are continuum-subtracted spectral comparisons between the observed and generic blue and red WR features. Generic spectra are taken from Crowther & Hadfield (2006) and have been scaled to the distance of NGC 1313, contributions expected from the WC4 (dashed line) and WN5–6 (dotted line) components are marked.

single generic WC4 star cannot reproduce the observed morphology and a WN5–6 contribution is required. The composite spectrum expected from a mixed population reproduces the observed features exceptionally well, such that we assign a population of 1 WC4 and 1 WN5–6 to #59. Similar results are obtained for NGC 1313 #67.

4.4 NGC 1313 #31 – the first WO star beyond the Local Group

In addition to identifying WN and WC stars within NGC 1313, our WR survey has revealed the signature of a WO star in one case.

In Fig. 7 we compare the spectrum of NGC 1313 #31 with LMC and SMC WO counterparts Sand 1 and 2 from Kingsburgh, Barlow & Storey (1995), clearly illustrating the presence of broad O VI λ3811–3834, C IV λ4658 and C IV λ5808 emission features. To our knowledge this represents the first detection of a WO star beyond the Local Group. Large linewidths [FWHM(λ5808) $\sim$ 100 Å]
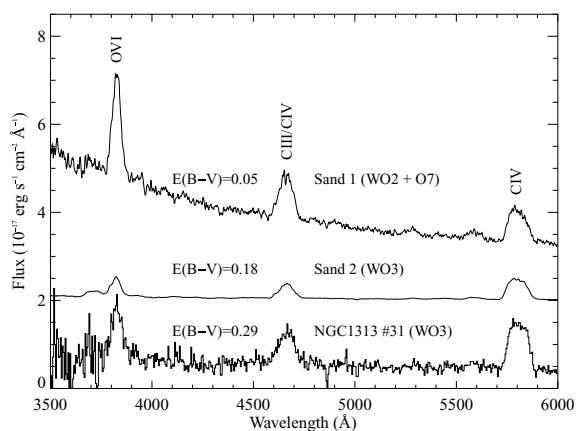
Figure 7. Dereddened spectral comparison between NGC 1313 #31 and Sand 1 (WO2 + O7) in the SMC and Sand 2 (WO3) in the LMC. The spectra for Sand 1 and 2 are taken from Kingsburgh et al. (1995) and have been scaled to the distance of NGC 1313 and extinction corrected by 0.05 and 0.18 mag, respectively. For clarity, individual spectra have been offset by 2×10^{-18} erg s^{-1} cm^{-1} Å^{-1}.

associated with #31 are apparent, and are observed to be comparable with those in Local Group WO counterparts.

For spectral classification we refer to the scheme of Crowther et al. (1998), where the ratio of the equivalent widths (W_λ) of O VI λ3811–3834 and O V λ5590 is used as the primary subtype discriminator. In our data, O V λ5590 is extremely weak and accurately classifying it based on this criterion is not possible. However, a classification can be made using the secondary line diagnostics O VI λ3811–3834 and C IV λ5808, which also suggests a WO3 classification.

NGC 1313 #31 is below the detection limit of our FORS1 B-band photometry, suggesting $m_B \geqslant 23.5$ mag. *HST*/ACS photometry of #31 yields $m_{F435W} = 23.4 \pm 0.01$ mag, $m_{F555W} = 23.8 \pm 0.01$ mag, $m_{F814W} = 25.4 \pm 0.05$ mag (Pellerin, private communication).

Single/binary WO stars are observed to exhibit $M_V \sim -3$ and -6 mag, respectively (Kingsburgh et al. 1995). For a total extinction $E_{B-V} = 0.29$ mag, we find $M_V \sim -5$ mag for #31, which is very bright for a single WO star, so #31 likely belongs to a binary system or small association.

5 THE GLOBAL WR CONTENT OF NGC 1313

Of the 94 WR candidates identified from VLT/FORS1 narrow-band imaging we have identified characteristic WR signatures in 70 regions from our spectroscopy to date. Using LMC template WR stars as local analogues, we have derived a global WR population of 84 stars, as summarized in Table 6.

5.1 Nature of candidates

In general, are the confirmed WR sources in NGC 1313 isolated WR stars, binaries or members of luminous stellar clusters/associations? One may expect the latter since our 0.8-arcsec slit width corresponds to a spatial scale of 15 pc at a distance of 4.1 Mpc.

It is well known that WC stars exhibit a larger λ4684 excess than their WN counterparts due to their intrinsically stronger emission features. Synthetic filter photometry of LMC template stars from Crowther & Hadfield (2006) suggests that a typical WC4 star in NGC 1313 should have $m_B \sim 23$ mag and $\Delta m = m_{\lambda4684} - m_B \sim -2$ mag. For WN stars, synthetic photometry suggests that single early-, mid- and late-type WN stars should exhibit photometric excesses of $\Delta m = -1.2, -0.6$ and -0.4 mag, respectively. Single WN2–4 stars within NGC 1313 would have an apparent B-band magnitude of $\sim$23 mag, whereas late-type WN stars should be slightly brighter with $m_B \sim 22$ mag.

In Fig. 8 we compare the actual λ4684 excess, Δm, with the B-band magnitude for our sample. As expected, the fainter candidates exhibit the largest excess ($\Delta m < -1.0$ mag) consistent with single or binary systems, where the WR emission is not strongly diluted by nearby stars. Sources with small photometric excess ($\Delta m \lesssim -0.5$ mag) correspond to the brighter end of our sample and are consistent with luminous clusters/associations, where the continua of nearby stars greatly dilute the WR emission.

Of course, intrinsic absolute magnitudes of WR stars are seen to display a large scatter (Crowther & Hadfield 2006), but based on Fig. 8 we conclude that three WCE sources (NGC 1313 #12, 41 and 81) within NGC 1313 are consistent with fairly isolated WC stars. The remaining 25 therefore belong to binary systems or lie within stellar clusters/associations. For the 50 WN sources, six WN2–4 and three WN7–9 stars have properties consistent with single, isolated WN stars.
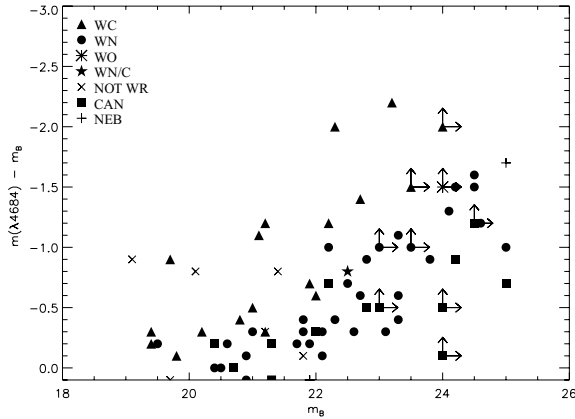
Figure 8. Comparison between Δm ($m_{\lambda 4684} - m_B$) and m_B for regions within NGC 1313. Regions which have been spectroscopically observed and subsequently classified or eliminated as WR regions are presented in the key. Also marked are candidates regions which still await spectroscopic follow-up.

For two sources known to host WR stars we find $\Delta m > 0.5$. Since $m_B \sim 19$ mag for these regions, both are consistent with luminous clusters/associations such that m_B is being contaminated by a population of stars that are intrinsically faint at $\lambda 4684$. For the six candidates which showed no evidence for WR features we find that the three confirmed late-type objects display significant photometric excesses ($\Delta m \geqslant -0.7$ mag). Such sources could be excluded from future spectroscopic surveys on the basis of their extremely red colours, $B - V \sim 1$ mag compared with $B - V \sim 0.1$ mag for genuine candidates. The three other non-WR detections only display negligible photometric excesses.

Of the 16 remaining candidate regions, eight display photometric excesses ($\Delta m \geqslant -0.3$ mag) consistent with confirmed WN sources. Indeed, three of these correspond to candidates for which WC stars were excluded since their spectra started longward of $\lambda 5000$. In the continuum-subtracted $\lambda 4684$ image (obtained by subtracting the $\lambda 4781$ frame from the $\lambda 4684$ image), the majority of the remaining candidates are bright and are comparable with genuine WN sources. Overall, we expect that 11 of the 16 remaining candidates will host WR stars, some of which appear multiple.

5.2 Completeness

How complete is our WR survey of NGC 1313? In Fig. 9 we compare a FORS1 $\lambda 4684$ narrow-band image with a continuum-subtracted $\lambda 4684$ image of the brightest star-forming region PES 1 (recall Table 4) which highlights the complexities involved in identifying WR candidates within crowded regions (see also Drissen, Moffat & Shara 1993).

Relatively isolated WR stars are readily identified but within the inner regions of PES 1 it is clear that some $\lambda 4686$ emission is spatially extended on our ground-based FORS1 images. The strong, bright emission associated with NGC 1313 #64, to the south of the H II regions, represents one of the most extreme examples. #64 is believed to host multiple WR stars based on the observed C IV $\lambda 5808$ line luminosity (Section 4.3). Spectroscopic observations were made with the slit aligned perpendicular to the extended emission, consequently ~ 50 per cent of the total flux may have been missed. The WR content of this region could therefore be in excess of six WR
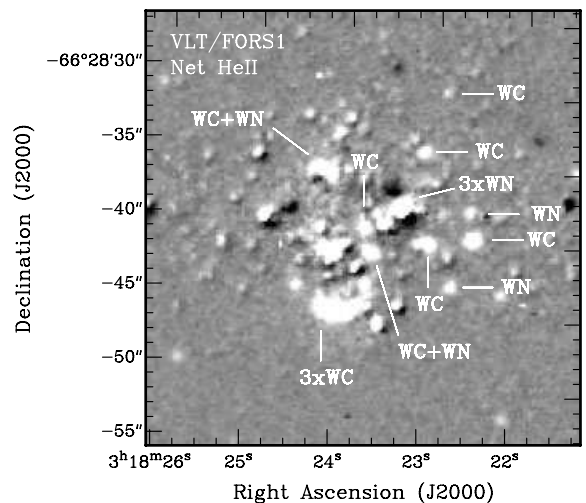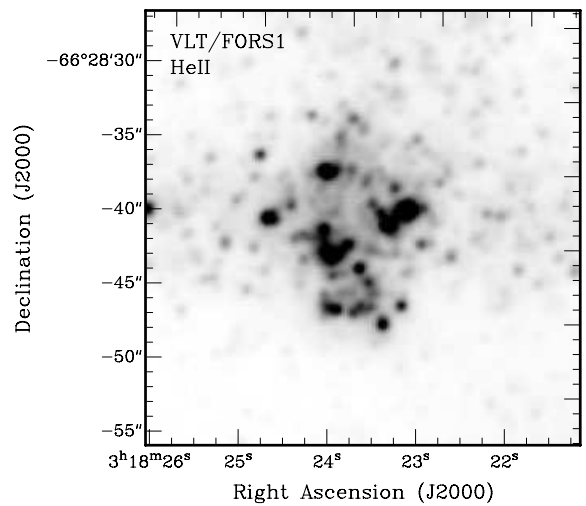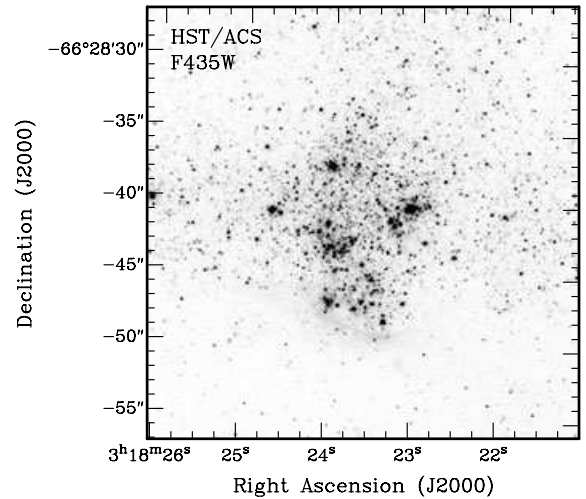
Figure 9. 30×30-arcsec^2 *HST*/ACS and VLT/FORS1 images of the bright star-forming region PES 1. At a distance of 4.1 Mpc the physical region illustrated equates to 600×600 pc. The $\lambda 4684$ excess sources, shown in white, which have been spectroscopically confirmed to host WR stars are marked. North is up and east is to the left-hand side on all images.

stars. Similar conclusions are reached for #65, for which images suggest ∼3 WR stars, but spectroscopy of #65 is not yet available.

Fig. 9 also shows a number of faint emission regions within PES 1, which may be genuine WR stars. In total, spectroscopic observations of PES 1 indicate a minimum of 17 WR stars comprising seven WN and 10 WC stars. The total WR content may be ∼26, significantly larger than the dozen WR stars seen within NGC 595 in M 33 (Drissen et al. 1993) and approaches the 41 WR stars identified within the much larger 30 Doradus region of the LMC (Breysacher, Azzopardi & Testor 1999).

Completeness issues of ground-based surveys are further highlighted by the *HST*/ACS F435W image of PES 1. The superior spatial resolution of *HST* is immediately apparent and #64 and 65 are clearly resolved into multiple stellar clusters/associations. If a core-collapse SN were to occur within either of these regions, even with *HST* it may not be possible to directly identify a WR progenitor.

Beyond PES 1, seven other candidate λ4684 emission regions appear spatially extended, even though observed line luminosities are consistent with a single star in each case. These sources have been indicated in Table A2. Allowing for the possibility that a few further λ4684 sources are WR stars (not listed in Table A2), we suggest that the total WR population of NGC 1313 is ∼115, 20 per cent of which are located within PES 1. Since most of the remaining candidates are consistent with WN stars, we infer $N(WC)/N(WN) = 0.4$.

5.3 The WR population

In Table 7 we compare the WR and O star content of NGC 1313 to several other Local Group, metal-poor [$\log(O/H) + 12 < 8.5$], galaxies. The WR content of NGC 1313 is similar to that observed in the LMC, yet its SFR is a factor of 3 higher. Consequently, the modest reduction in metallicity of NGC 1313 relative to the LMC either causes fewer O stars to advance to the WR phase, or results in shorter WR lifetimes. The WR content of NGC 1313 is more comparable to that of IC 10, at a similar metallicity, once their relative SFR are taken into account (see Table 7).

Over the last few decades WR populations have been well sampled in a wide variety of environments and it is well known that the distribution of WC to WN stars is dependant on metallicity (Massey, Olsen & Parker 2003). Large WC/WN ratios are observed in extremely metal-rich environments, e.g. $N(WC)/N(WN) \sim 1$ in M 83 (Hadfield et al. 2005), while small ratios are observed in metal-poor environments, e.g. $N(WC)/N(WN) = 0.2$ in the LMC (Breysacher et al. 1999). Based on the low metallicity of NGC 1313 one would expect $N(WC)/N(WN) \sim 0.1$. Here, we estimate a significantly higher subtype ratio of ∼0.6 (or ∼0.4 if we adopt a WN subtype for the majority of our remaining candidates). This is inter-
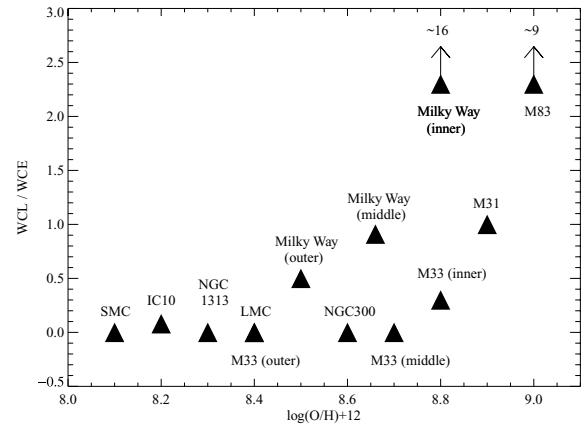
Figure 10. The distribution of late (WC7–9) to early (WC4–6) carbon-sequence WR stars in NGC 1313 and other well-studied galaxies versus metal content. Data are taken from Massey & Johnson (1998), Breysacher et al. (1999), Massey et al. (2003), Crowther et al. (2003), Abbott et al. (2004), Hadfield et al. (2007), Crowther et al. (2007) and the present study.

mediate between that observed in the outer, subsolar regions of M 33 where $N(WC)/N(WN) \sim 0.35$ (Massey & Johnson 1998) and the inner region of NGC 300 for which $N(WC)/N(WN) \sim 0.7$ (Crowther et al. 2007).

5.4 Using the WC content as a proxy for metallicity

It has long been recognized that late-type WC stars are preferentially found within metal-rich environments. For example, in the Milky Way WC9 stars are universally located within the inner, metal-rich regions (Conti & Vacca 1990) and an overwhelming WC8–9 population is seen in M 83 (Hadfield et al. 2005). Conversely, metal-poor WC stars in the SMC and LMC are predominantly early-types (Breysacher et al. 1999). Crowther et al. (2002) attributed the dominance of early WC subtypes in low-metallicity environments to weak WC winds, since the C III λ5696 classification line scales very sensitively with wind density. This is further supported by the fact that the WC population of NGC 1313 is comprised solely of early-type WC and WO stars.

In Fig. 10 we show the subtype ratio of WC7–9 to WC4–6 stars in NGC 1313 and other nearby galaxies. At high metallicities [$\log(O/H) + 12 \geqslant 8.8$], wind densities are sufficiently high to reveal strong C III λ5696 emission in the majority of WC stars, such that late WC subtypes dominate the population (e.g. M 83). For intermediate metallicities [$\log(O/H) + 12 \sim 8.5$–8.8], the WC population is composed of a mixture of early and late WC subtypes,

Table 7. WR and O star populations of NGC 1313 and several metal-poor [$\log(O/H) + 12 < 8.5$] Local Group galaxies.

Galaxy	$\log(O/H)$ +12	$N(WR)$	$N(WR)/$ $N(O)$ (10^{-2})	$N(WC)/$ $N(WN)$	SFR $(M_\odot\ yr^{-1})$	Reference
LMC	8.37	134	3.0	0.2	0.22	1, 2
IC 10	8.26	⩾26	⩾0.6	1.3	0.20	3, 5
NGC 1313	8.23	∼115	∼0.9	∼0.4	0.64	6
SMC	8.13	12	1.5	0.1	0.04	1, 4

References: (1) Kennicutt et al. (1995); (2) Breysacher et al. (1999); (3) Crowther et al. (2003); (4) Massey et al. (2003); (5) Leroy et al. (2006); (6) this paper.

as observed for the solar neighbourhood. For metal-poor galaxies [log(O/H) + 12 $\lesssim$ 8.5] wind densities are low, and are insufficient to produce late-type WC stars. Consequently, galaxies such as the SMC and NGC 1313 only host early-type WC and their high-temperature WO counterparts.

Exceptions to this general trend do occur. In the metal-poor galaxy IC 10 [log(O/H)+12 = 8.26] Crowther et al. (2003) identify one of the 14 WC stars as a WC7 subtype. At high metallicities a small fraction of early WC subtypes are also seen (e.g. M 83). Nevertheless, it appears that the dominant WC subtype may serve as a crude metallicity diagnostic for integrated stellar populations, e.g. late WC subtypes for NGC 1365 at high-metallcity (Phillips & Conti 1992) and early WC subtype for NGC 3125 at low metallicity (Hadfield & Crowther 2006).

5.5 The origin of nebula He II λ4686

The rarity of H II regions which show nebular He II λ4686 among Local Group galaxies (Garnett et al. 1991) illustrates the significance of such regions within NGC 1313.

The association of nebular He II λ4686 emission with WNE and WO stars (e.g. NGC 1313 #19) in low-metallicity environments argues in favour of WR stars being the source of the high ionization. It has long been predicted that the hard ionizing flux output of a WR star is dependant on wind density (Schmutz, Leitherer & Gruenwald 1992). Model atmospheres of Smith, Norris & Crowther (2002) predict that low wind densities favour transparent winds such that only weak winds are expected to produce a significant He$^+$ continuum below 228 Å. Consequently, dense winds associated with most WC and WN stars are not expected to produce strong He$^+$ ionizing radiation.

Since mass-loss rates of WR stars are predicted (Vink & de Koter 2005), and observed to scale with metallicity (Crowther et al. 2002), it is expected that He II nebulae are preferentially associated with WR stars in metal-poor galaxies. Smith et al. (2002) predict that for WNE stars the He$^+$ continuum increases from log Q_2 = 41.2 at $Z = Z_\odot$ to 48.3 for $Z = 0.2 \, Z_\odot$. In metal-rich environments WR stars would not be capable of ionizing He$^+$. Indeed, five of the six WR stars which exhibit nebular He II are in galaxies with log(O/H) + 12 < 8.4 (Table 5), with the association increasing from less than 0.3 per cent in the Milky Way (e.g. Sand 4, Polcaro et al. 1995) to 100 per cent in IC 1613 which is a factor of 10 lower in metallicity (Kingsburgh & Barlow 1995).

6 SUMMARY AND CONCLUSIONS

We present the results of an imaging and spectroscopic survey of the WR content of the nearby galaxy NGC 1313. From narrow-band λ4684 and λ4781 images we have identified 94 candidate He II emission regions of which 82 have been spectroscopically observed. Broad WR emission has been identified within 70 regions, with only six candidates failing to show stellar/nebular He II λ4686 emission.

A nebular analysis of several H II regions within the galaxy confirms that NGC 1313 has a metal content [log(O/H) + 12 = 8.23 ± 0.06] intermediate between the SMC and LMC and equivalent to that of IC 10. Using template LMC WR stars, we estimate N(WR) = 84, with N(WC)/N(WN) $\sim$ 0.6 from spectroscopy. The 51 WN stars are evenly distributed amongst early and late subtypes and include a rare WN/C4 transition star. The 33 WC stars are exclusively early-type stars, one of which we assign a WO classification. Indeed, NGC 1313 #31 represents the first WO star identified beyond the Local Group.

Photometry of the remaining candidates, plus a number of additional sources identified from spatially extended λ4684 emission (primarily within PES 1), are mostly consistent with WN subtypes. We suggest a total WR content of N(WR) $\sim$ 115 for NGC 1313; a factor of 4 higher than that observed in IC 10 for which the SFR is three times lower. The bright star-forming region PES 1 hosts 20 per cent of the entire WR content of NGC 1313, higher than that observed in NGC 595 in M 33 despite a comparable Hα luminosity. Globally N(WC)/N(WN) $\sim$ 0.4, substantially higher than that of the LMC for which N(WC)/N(WN) = 0.2.

Late-type WC stars are notably absent in NGC 1313, a common feature of metal-poor galaxies within the Local Group. Indeed, one may infer the metallicity of a spatially unresolved WR galaxy based on the dominant WC subtype. If the spectral appearance is dominated by late-type WC stars then one would infer log(O/H) + 12 $\gtrsim$ 8.8. Conversely, a dominant early-type WC appearance suggests log(O/H) + 12 $\lesssim$ 8.5.

In addition, we have identified strong nebular He II λ4686 in three regions within NGC 1313. For NGC 1313 #19, the nebular emission is accompanied by broad He II emission (consistent with an WNE star), only the sixth case believed to be ionized by a WR star. For the other two regions, one is consistent with shock ionization, most probably an SNR, whereas the ionizing source of NGC 1313 #6 may possibly be a X-ray source, similar to that inferred for N44C within the LMC.

REFERENCES

Abbott J. B., Crowther P. A., Drissen L., Dessart L., Martin P., Boivin G., 2004, MNRAS, 350, 552
Breysacher J., Azzopardi M., Testor G., 1999, A&AS, 137, 117
Colbert E. J. M., Petre R. S. E. M., Ryder S. D., 1995, ApJ, 446, 177
Conti P. S., Vacca W. D., 1990, AJ, 100, 2
Crowther P. A., 2007, A&AR, 45, 177
Crowther P. A., Hadfield L. J., 2006, A&A, 449, 711
Crowther P. A., Smith L. J., Willis A. J., 1995, A&A, 304, 269
Crowther P. A., De Marco O., Barlow M. J., 1998, MNRAS, 296, 367
Crowther P. A., Dessart L., Hillier D. J., Abbott J., Fullerton A. W., 2002, A&A, 392, 653
Crowther P. A., Drissen L., Abbott J. B., Royer P., Smartt S. J., 2003, A&A, 404, 483
Crowther P. A., Carpano S., Hadfield L. J., Pollock A. M. T., 2007, A&A, 469, L31
Drissen L., Moffat A. F. J., Shara M. M., 1993, A&A, 105, 1400
Friedli D., Benz W., Kennicutt R., 1994, ApJ, 430, 105
Garnett D., Kennicutt R. C., Chu Y. H., Skillman E. D., 1991, AJ, 373, 458
Garnett D., Galarza V. C., Chu Y.-H., 2000, AJ, 545, 251
Hadfield L. J., Crowther P. A., 2006, MNRAS, 368, 1822
Hadfield L. J., Crowther P. A., Schild H., Schmutz W., 2005, A&A, 439, 265
Hadfield L. J., van Dyk S. D., Morris P. W., Smith J. D., Marston A. P., Peterson D. E., 2007, MNRAS, 376, 248
Hummer D., Storey P. J., 1987, MNRAS, 224, 801
Kennicutt R. C., 1984, ApJ, 287, 116
Kennicutt R. C., 1998, ARA&A, 36, 189
Kennicutt R. C., Kent S. M., 1983, AJ, 88, 1094
Kennicutt R. C., Bresolin F., Bomans D. J., Bothun G. D., Thompson I., 1995, AJ, 109, 594
Kingsburgh R., Barlow M. J., 1995, A&A, 295, 171

Kingsburgh R., Barlow M. J., Storey P., 1995, A&A, 295, 75
Landolt A. U., 1992, AJ, 104, 340
Larsen S., 2004, A&A, 416, 537
Leroy A., Bolatto A., Walter F., Blitz L., 2006, ApJ, 643, 825
Marcelin M., Gondoin P., 1983, A&AS, 51, 3538
Massey P., Johnson O., 1998, ApJ, 505, 793
Massey P., Olsen K. A. G., Parker J. W., 2003, PASP, 115, 1265
Méndez B., Davis M., Moustakas J., Newman J., Madore B. F., Freedman W. L., 2002, AJ, 124, 213
Miller S., Schlegel E. M., Petre R., Colbert E., 1998, AJ, 116, 1657
Nazé Y., Rauw G., Manfroid J., Chu Y.-U., Vreux J.-M., 2003a, A&A, 408
Nazé Y., Rauw G., Manfroid J., Chu Y.-U., Vreux J.-M., 2003b, A&A, L13
Pagel B. E. J., Edmunds M. G., Smith G., 1980, MNRAS, 193, 219
Pellerin A., Meyer M., Harris J., Calzetti D., 2007, AJ, 658, L87
Phillips A., Conti P., 1992, ApJ, 385, L91
Polcaro V. F., Rossi C., Norci L., Viotti R., 1995, A&A, 303, 211
Russell S. C., Dopita M., 1990, ApJS, 74, 93
Ryder S. D., Dopita M. A., 1994, ApJ, 430, 142
Schaerer D., Vacca W. D., 1998, ApJ, 497, 618
Schaerer D., Contini T., Pindao M., 1999, A&A, 341, 399
Schild H., Crowther P. A., Abbott J. B., Shmutz W., 2003, A&A, 397, 859
Schlegel D. J., Finkbeiner D. P., Davis M., 1998, ApJ, 500, 525
Schmutz W., Leitherer C., Gruenwald R., 1992, PASP, 104, 1164
Seaton M. J., 1979, MNRAS, 187, 73P
Smith L. F., Shara M. M., Moffat A. J., 1990, ApJ, 348, 471
Smith L. F., Shara M. M., Moffat A. J., 1996, MNRAS, 281, 229
Smith L. F., Norris R. F. P., Crowther P. A., 2002, MNRAS, 337, 1309
Smith R. C., Kirshner R. P., Blair W. B., Long K. S., Winkler P. F., 1993, ApJ, 407, 564
van der Hucht K. A., 2006, A&A, 458, 453
Vink J. S., de Koter A., 2005, A&A, 442, 587
Walsh J. R., Roy J. R., 1997, MNRAS, 288, 726

APPENDIX A: CATALOGUES

Here we present catalogues of H II regions observed in NGC 1313 along with candidate He II emission regions identified from VLT/FORS1 narrow-band imaging.

Table A1. Catalogue of H II regions observed with NGC 1313.

| # | α | δ | $E(B-V)$ | H II association | |
	(J2000)			PES	W&R
H1	03:17:57.2	−66:29:43.6	0.22	–	–
H2	03:17:57.3	−66:31:39.5	0.20	–	–
H3	03:18:05.3	−66:30:27.8	0.19	6	20
H4	03:18:05.3	−66:30:53.7	0.28	–	–
H5	03:18:07.8	−66:31:21.2	0.26		23
H6	03:18:24.8	−66:31:46.3	0.26	–	–
H7	03:18:25.9	−66:27:43.0	0.35	–	–
H8	03:18:33.3	−66:27:42.1	0.56	–	–
H9	03:18:40.9	−66:29:30.5	0.24	10	3

Table A2. Catalogue of candidate He II emission regions within NGC 1313. Association with H II regions identified by (W&R, Walsh & Roy 1997) and (PES, Pagel et al. 1980) is also given. Note that values in parenthesis correspond to candidates which reside close to W&R and PES regions. We present line properties and spectral types for those regions which have been classified via follow-up spectroscopy. Sources believed to host multiple WRs based on the observed line flux or appearance on the continuum-subtracted λ4684 image have been identified. Regions which are awaiting follow-up spectroscopy have been labelled WN? or NON-WR? depending on their photometric excess and appearance on the continuum-subtracted λ4684 image. Deprojected distances are expressed as a fraction of the Holmberg radius $\rho_0 = 4.6$ arcmin $= 5.5$ kpc. Dereddened line fluxes have been derived assuming $E_{B-V} = 0.29$ mag and are expressed in erg s^{-1} cm^{-2}. The number of WR stars in each source is estimated using the line luminosity calibrations of Crowther & Hadfield (2006) and a distance modulus of 28.08 mag (Méndez et al. 2002).

#	α	δ (J2000)	ρ/ρ_0	H II association W&R	PES	m_B (mag)	m_{4684} (mag)	Δm (mag)	$F(\lambda4650)+F(\lambda4686)$	$L(\lambda4650)+L(\lambda4686)$	$F(\lambda5808)$	$L(\lambda5808)$	Spectral type	Remarks
1	03:17:40.3	−66:31:30.4	1.25			22.5	21.9	−0.7		No data available			WNE	⩾1WN
2	03:17:41.0	−66:31:37.1	1.24			22.7	21.2	−1.4	No blue data		1.1×10^{-15}	4.9×10^{36}	WC4–5	
3	03:17:43.6	−66:31:15.2	1.13			22.1	21.8	−0.3	1.6×10^{-16}	9.1×10^{35}			WN7–9	
4	03:17:46.0	−66:31:47.2	1.09			21.3	21.1	−0.2	No blue data					NON-WR?
5	03:17:47.7	−66:29:45.8	0.94			21.8	21.8	0.0						NON-WR
6	03:17:47.7	−66:29:37.4	0.95			25.0	23.3	−1.7						Neb He II
7	03:17:57.8	−66:33:05.1	0.93	(27)		20.4	20.4	0.0	2.6×10^{-16}	1.5×10^{36}			WN7–9	
8	03:17:58.0	−66:33:07.9	0.93	27		20.1	20.3	0.2	2.5×10^{-16}	1.4×10^{36}			WN7–9	
9	03:17:59.3	−66:30:12.0	0.56			23.1	22.8	−0.3	7.2×10^{-17}	4.0×10^{35}			WN2–4	
10	03:17:59.7	−66:30:06.3	0.54	22		19.4	19.2	−0.3	1.5×10^{-15}	8.6×10^{36}	1.7×10^{-15}	7.3×10^{36}	WC4–5	2 × WC?
11	03:18:01.0	−66:29:29.8	0.50			22.5	21.7	−0.8	3.7×10^{-16}	2.1×10^{36}	5.7×10^{-16}	2.5×10^{36}	WN5–6/C4	
12	03:18:01.9	−66:30:09.5	0.47			22.3	20.3	−2.0	1.5×10^{-15}	8.6×10^{36}	1.0×10^{-15}	4.5×10^{36}	WC4–5	Mulitple WRs?
13	03:18:02.7	−66:32:51.6	0.79			22.7	22.2	−0.6	2.5×10^{-16}	1.4×10^{36}			WN7–9	
14	03:18:02.8	−66:30:14.9	0.44	21	6	17.1	17.8	0.8	4.7×10^{-16}	2.7×10^{36}			WN5–6?	Mulitple WRs?
15	03:18:03.7	−66:32:32.9	0.71	25	7	20.8	20.5	−0.4	No blue data		8.7×10^{-16}	3.8×10^{36}	WC4–5	
16	03:18:03.7	−66:30:23.1	0.42			21.2	20.9	−0.3	9.1×10^{-16}	5.1×10^{36}	9.0×10^{-16}	3.8×10^{36}	WC4–5	Mulitple WRs?
17	03:18:03.9	−66:30:19.5	0.41			—	—	—	1.9×10^{-15}		1.1×10^{37}		WN	Multiple WRs?
18	03:18:04.0	−66:30:01.8	0.39			24.1	22.8	−1.3	1.2×10^{-16}	6.8×10^{35}			WN7–9	
19	03:18:04.4	−66:32:46.6	0.74			23.8	23.0	−0.9	1.4×10^{-16}	8.0×10^{35}			WN2–4	
20	03:18:04.4	−66:30:21.2	0.39			22.0	21.4	−0.6	3.4×10^{-16}	1.9×10^{36}	3.3×10^{-16}	1.4×10^{36}	WC4–5	
21	03:18:04.9	−66:30:27.0	0.38	20	5	20.6	20.8	0.2	1.7×10^{-16}	9.4×10^{35}			WN7–9	
22	03:18:05.2	−66:30:26.2	0.37	20	5	17.8	18.8	1.0					WN7–9	
23	03:18:06.1	−66:30:38.0	0.36			23.3	22.9	−0.4	2.0×10^{-16}	1.1×10^{36}			WN2–4	
24	03:18:06.7	−66:30:21.5	0.32			21.0	20.7	−0.3	2.4×10^{-16}	1.3×10^{36}			WN7–9	
25	03:18:09.1	−66:30:04.6	0.22			24.2	22.7	−1.5	1.8×10^{-16}	1.0×10^{36}			WN7–9	
26	03:18:10.9	−66:31:07.7	0.32			19.1	18.3	−0.9						Late
27	03:18:11.1	−66:29:34.8	0.16			21.2	21.0	−0.3						NON-WR
28	03:18:11.7	−66:28:42.2	0.28			>23	>22.5	< −0.5						WN?
29	03:18:12.7	−66:30:54.2	0.25			23.3	22.3	−1.1	2.0×10^{-16}	1.1×10^{36}			WN2–4	
30	03:18:13.4	−66:32:16.0	0.53			21.9	21.7	−0.2	7.3×10^{-17}	4.1×10^{35}			WN7–9	
31	03:18:13.5	−66:29:30.9	0.10			>24	23.3	< −1	2.9×10^{-16}	1.7×10^{36}	5.7×10^{-16}	2.5×10^{36}	WO3	
32	03:18:13.6	−66:32:17.1	0.54			22.3	21.9	−0.4	1.1×10^{-16}	6.0×10^{35}			WN7–9	
33	03:18:13.9	−66:30:24.1	0.13				Extended		4.7×10^{-16}	2.6×10^{36}			WN2–4	3 × WN?
34	03:18:14.2	−66:29:55.9	0.05			22.0	21.7	−0.3						WN?
35	03:18:14.9	−66:30:21.5	0.11	17		19.4	19.2	−0.2	9.0×10^{-16}	5.1×10^{36}	8.0×10^{-16}	3.5×10^{36}	WC4–5	
36	03:18:15.0	−66:29:10.4	0.15			20.1	19.3	−0.8						Late
37	03:18:15.4	−66:29:54.0	0.01				Extended		1.1×10^{-15}	6.0×10^{36}	7.8×10^{-16}	3.5×10^{36}	WC4–5	

Table A2 – *continued*

#	α	δ (J2000)	ρ/ρ₀	W&R	PES	m_B (mag)	m_{4684} (mag)	Δm (mag)	$F(\lambda4650)+$ $F(\lambda4686)$	$L(\lambda4650)+$ $L(\lambda4686)$	$F(\lambda5808)$	$L(\lambda5808)$	Spectral type	Remarks
38	03:18:16.6	−66:28:45.1	0.24			19.7	19.8	0.1						NON-WR
39	03:18:17.2	−66:28:36.5	0.28			20.9	20.8	−0.1	1.7×10^{-16}	9.6×10^{35}			WN7–9	
40	03:18:17.6	−66:30:08.9	0.10			24.5	22.9	−1.6	3.1×10^{-16}	1.7×10^{36}			WN2–4	
41	03:18:17.8	−66:29:03.8	0.19	13	9	23.2	21.0	−2.2	6.3×10^{-16}	3.5×10^{36}	5.9×10^{-16}	2.6×10^{36}	WC4–5	
42	03:18:18.2	−66:29:05.8	0.19	13	9		Extended		8.7×10^{-16}	4.9×10^{36}	6.1×10^{-16}	2.7×10^{36}	WC4–5	
43	03:18:19.8	−66:28:43.4	0.29	12	11		Extended							NON-WR?
44	03:18:20.5	−66:30:28.6	0.22			24.0	22.5	−1.5	1.3×10^{-16}	7.2×10^{35}			WN2–4	
45	03:18:20.7	−66:28:29.8	0.35			25.0	24.0	−1.0	2.3×10^{-16}	1.3×10^{36}			WN2–4	
46	03:18:21.0	−66:28:37.4	0.33			21.7	21.5	−0.2	1.3×10^{-16}	7.6×10^{35}			WN2–4	
47	03:18:21.7	−66:29:44.7	0.21			21.8	21.5	−0.3	7.8×10^{-17}	4.4×10^{35}			WN7–9	
48	03:18:21.9	−66:30:06.3	0.22			21.1	20.0	−1.1	1.5×10^{-15}	8.6×10^{36}	1.4×10^{-15}	6.0×10^{36}	WC4–5	2 × WC?
49	03:18:21.9	−66:29:47.9	0.22			20.2	19.8	−0.3	6.7×10^{-16}	3.8×10^{36}	4.6×10^{-16}	2.0×10^{36}	WC4–5	Multiple WRs?
50	03:18:22.3	−66:28:42.3	0.34		(1)	22.2	21.0	−1.2	1.1×10^{-15}	6.2×10^{36}	9.8×10^{-16}	4.2×10^{36}	WC4–5	
51	03:18:22.3	−66:28:40.5	0.35		(1)	>23	>22	< −1	1.9×10^{-16}	1.1×10^{36}			WN2–4	
52	03:18:22.5	−66:30:03.8	0.24			22.8	21.9	−0.9	2.3×10^{-16}	1.3×10^{36}			WN2–4	
53	03:18:22.5	−66:28:45.6	0.34		(1)	>23.5	>22.5	< −1	2.4×10^{-16}	1.4×10^{36}			WN2–4	
54	03:18:22.6	−66:29:41.4	0.24			−	−	−						WN?
55	03:18:22.7	−66:28:20.2	0.41				Extended		1.8×10^{-16}	1.0×10^{36}			WN2–4	
56	03:18:22.8	−66:28:42.7	0.35		(1)	>23.5	22:	>1.5	1.7×10^{-16}	9.3×10^{35}	1.3×10^{-16}	5.6×10^{35}	WC4–5	
57	03:18:22.8	−66:28:36.1	0.37		(1)	21.9	21.2	−0.7	5.6×10^{-16}	3.1×10^{36}	5.5×10^{-16}	2.4×10^{36}	WC4–5	
58	03:18:23.1	−66:28:40.1	0.37	10	1		Extended		8.3×10^{-16}	4.7×10^{36}			WN5–6?	3 × WN?
59	03:18:23.5	−66:28:43.4	0.37	10	1	20.4	20.9	0.5			7.8×10^{-16}	3.4×10^{36}	WC4–5 + WN5–6?	
60	03:18:23.5	−66:28:41.4	0.37	10	1		Extended		4.7×10^{-16}	2.7×10^{36}	8.3×10^{-16}	3.7×10^{36}	WC4–5	
61	03:18:23.6	−66:32:57.9	0.74	28		21.2	20.0	−1.2	No blue data		2.1×10^{-15}	9.4×10^{36}	WC4–5	3 × WC?
62	03:18:23.7	−66:32:57.7	0.74	28		21.0	20.5	−0.5	No blue data		1.1×10^{-15}	4.6×10^{36}	WC4–5	
63	03:18:23.8	−66:28:21.3	0.43			22.8	22.3	−0.5						WN?
64	03:18:23.9	−66:28:47.2	0.37	10	1	19.7	18.8	−0.9	4.2×10^{-15}	2.4×10^{37}	2.4×10^{-15}	1.1×10^{37}	WC4–5	3 × WC?
65	03:18:23.9	−66:28:42.7	0.38	10	1		Extended							Multiple WN?
66	03:18:23.9	−66:28:37.9	0.39	10	1		Extended		1.5×10^{-15}	8.3×10^{36}	1.7×10^{-15}	7.7×10^{36}	WC4–5	2 × WC?
67	03:18:24.1	−66:28:37.3	0.40	10	1		Extended				1.1×10^{-15}	4.9×10^{36}	WC4–5 + WN5–6?	
68	03:18:25.7	−66:28:50.6	0.41			24.2	23.3	−0.9						WN?
69	03:18:26.7	−66:27:56.7	0.56			21.4	20.6	−0.8						Late
70	03:18:27.1	−66:28:24.5	0.51			23.3	22.7	−0.6	8.4×10^{-17}	4.7×10^{35}			WN2–4	
71	03:18:27.9	−66:28:42.8	0.49	9		>23	21.7	< −1.3	1.9×10^{-16}	1.1×10^{36}			WN2–4	
72	03:18:27.9	−66:28:41.9	0.49	9		20.3	20.5	0.2	7.1×10^{-17}	4.0×10^{35}			WN7–9	
73	03:18:28.6	−66:28:48.6	0.50	9		20.5	20.6	0.0	1.5×10^{-16}	8.6×10^{35}			WN7–9	
74	03:18:29.2	−66:28:42.8	0.53	(9)		21.9	22.0	0.0					SNR?	Neb He II
75	03:18:33.1	−66:34:04.3	1.10			>24.5	23.3	< −1.2	No blue data				WN?	
76	03:18:34.4	−66:29:18.2	0.65			22.6	22.3	−0.3	2.3×10^{-16}	1.3×10^{36}			WN2–4	
77	03:18:35.3	−66:29:21.7	0.68			20.6	20.4	−0.2	2.0×10^{-16}	1.1×10^{36}			WN7–9	
78	03:18:35.8	−66:29:36.6	0.69			22.0	22.2	0.2	2.3×10^{-16}	1.3×10^{36}			WN2–4	
79	03:18:35.9	−66:28:38.9	0.74			24.6	23.4	−1.2	1.4×10^{-16}	8.1×10^{35}			WN2–4	

Table A2 – *continued*

#	α (J2000)	δ	ρ/ρ_0	W&R	PES	m_B (mag)	m_{4684} (mag)	Δm (mag)	$F(\lambda 4650)+F(\lambda 4686)$	$L(\lambda 4650)+L(\lambda 4686)$	$F(\lambda 5808)$	$L(\lambda 5808)$	Spectral type	Remarks
				H II association										
80	03:18:36.5	−66:29:31.0	0.72	5	3	25.0	24.3	−0.7						WN?
81	03:18:36.7	−66:29:32.0	0.72	5	3	>24	21.6	<−2	5.4×10^{-18}	3.0×10^{34}	7.7×10^{-16}	3.4×10^{36}	WC4-5	
82	03:18:36.9	−66:29:24.1	0.73			>24	>23.5	<−0.5	No blue data					WN?
83	03:18:36.9	−66:29:15.1	0.74			21.8	21.5	−0.4	1.1×10^{-16}	6.3×10^{35}			WN7-9	NON-WR?
84	03:18:37.1	−66:29:18.9	0.74			20.4	20.2	−0.2						
85	03:18:37.5	−66:29:34.8	0.75	5	3	19.0	19.9	0.9	2.4×10^{-16}	1.4×10^{36}			WN7-9	Multiple WRs?
86	03:18:38.4	−66:28:46.5	0.81	(6)		22.2	21.5	−0.6	No blue data					WN?
87	03:18:38.6	−66:29:09.3	0.80			>24	23.9	<−0.1						NON-WN?
88	03:18:41.0	−66:30:08.9	0.87	4		19.8	19.7	−0.1	No blue data		1.4×10^{-15}	6.1×10^{36}	WC4-5	2 × WC?
89	03:18:41.5	−66:30:19.7	0.89			21.3	21.4	0.1						NON-WR?
90	03:18:41.9	−66:29:31.0	0.90	3	10	19.5	19.3	−0.2	1.8×10^{-16}	1.0×10^{36}			WN7-9	Multiple WRs?
91	03:18:42.0	−66:29:41.9	0.90			22.1	21.9	−0.1	9.0×10^{-17}	5.1×10^{35}			WN7-9	
92	03:18:42.4	−66:29:33.0	0.92	3	10	20.9	21.0	0.1	1.2×10^{-16}	6.7×10^{35}			WN7-9	
93	03:18:42.5	−66:29:41.4	0.92			20.7	20.7	0.0						
94	03:18:44.5	−66:29:08.5	1.00			22.2	21.2	−1.0	1.1×10^{-16}	6.3×10^{35}			WN7-9	NON-WR?

SUPPLEMENTARY MATERIAL

The following supplementary material is available for this article.

Figure B1. Master finding chart indicating the 94 candidates identified (triangles) and positions of individual finding charts (1–9). North and east are marked on this $\lambda 4684$ FORS1 image of NGC 1313 (6.8×6.8 arcmin^2).

Figure B2. Finding chart 1. North and east are marked on this $\lambda 4684$ narrow-band FORS1 image. WR candidates and the image scale are also indicated.

Figure B3. Finding chart 2. WR candidates and the image scale are indicated. The bright star-forming region PES 1 is identified on this $\lambda 4684$ narrow-band FORS1 image, and magnified in the inset panel in the top right-hand corner of the image. North and east are indicated.

Figure B4. Finding chart 3. North is up and east is to the left on the FORS1 $\lambda 4684$ narrow-band image. WR candidates and the image scale are indicated.

Figure B5. Finding chart 4. North is up and east is to the left on the FORS1 $\lambda 4684$ narrow-band image. WR candidates and the image scale are indicated.

Figure B6. Finding chart 5. North is up and east is to the left on the FORS1 $\lambda 4684$ narrow-band image. WR candidates and the image scale are indicated.

Figure B7. Finding chart 6. North is up and east is to the left on the FORS1 $\lambda 4684$ narrow-band image. WR candidates and the image scale are indicated.

Figure B8. Finding chart 7. North is up and east is to the left on the FORS1 $\lambda 4684$ narrow-band image. WR candidates and the image scale are indicated.

Figure B9. Finding chart 8. North is up and east is to the left on the FORS1 $\lambda 4684$ narrow-band image. WR candidates and the image scale are indicated.

Figure B10. Finding chart 9. WR candidates, north and east and the image scale are indicated on the FORS1 $\lambda 4684$ narrow-band image.

This material is available as part of the online paper from: http://www.blackwell-synergy.com/doi/abs/10.1111/j.1365-2966.2007.12284.x
(this link will take you to the article abstract).

Please note: Blackwell Publishing are not responsible for the content or functionality of any supplementary materials supplied by the authors. Any queries (other than missing material) should be directed to the corresponding author for the article.

This paper has been typeset from a TeX/LaTeX file prepared by the author.